

How do the strongest radio pulses from thunderstorms relate to lightning flashes?

Abram R. Jacobson

Space and Atmospheric Sciences Group
Mail Stop D466
Los Alamos National Laboratory
Los Alamos, New Mexico 87545 USA
tel (505)667-9656 fax (505)665-7395
ajacobson@lanl.gov

This document is being submitted to the American Geophysical Union's Journal of Geophysical Research for possible publication. If the document is ultimately published by JGR, copyright will pass to the AGU. Until its formal publication in a peer-reviewed journal, this document may not be formally cited, and this document is being made available for informal technical communication and discussion only. All formal citation of this document must await its publication in final form in a peer-reviewed journal.

Abstract

We present a statistical analysis of thunderstorm radiofrequency and optical data from the FORTE satellite to examine the relationship of strong radiofrequency pulsed emissions to more conventional signals from lightning. The study is built on a FORTE database of intracloud, pulsed radio signals from storms whose geolocation is provided either by coincidence with the FORTE optical imager or by coincidence with ground-based lightning-detection arrays. We show statistically that intracloud radio emissions with peak power > 40 kW in the FORTE low band (26-48 MHz) have unique characteristics compared to weaker emissions, including: Occurring either in isolation or at the start of leader progression, but never within a progressing leader; occurring without light emission detectable by FORTE; occurring in frequent association with a rapid (10 μ s) relaxation of the electric charge; and being followed by an upward-progressing leader, in the cases where a leader is initiated. These strong intracloud radio pulses appear to be associated with an intracloud discharge process that is physically distinct from conventional leader progression.

1. Introduction

Both legacy [*Le Vine*, 1980; *Willett et al.*, 1989] and recent [*Jacobson*, 2003; *Jacobson and Light*, 2003; *Light and Jacobson*, 2003; *Smith et al.*, 1999; *Thomas et al.*, 2001] studies of radiofrequency (RF) emissions from thunderstorms have noted a distinct class of very powerful pulses emitted from the upper troposphere. This pulse can be accompanied by a “Narrow Bipolar Event” or NBE [*Smith et al.*, 1999], which is a large-scale discharge (tens of coulomb-km) of intracloud (IC) charge structures occurring in ~ 10 μ s. It has also been observed that these strong RF pulses are less likely to be accompanied by detectable light output than are weaker RF pulses [*Light and Jacobson*, 2003]. These strong RF pulses are routinely recorded by radiofrequency sensors aboard the GPS constellation [*Suszcynsky et al.*, 2000a] and are thus a candidate signature for global, near-real-time monitoring of thunderstorm activity using that constellation. As a remote-sensing signature, these strong RF pulses offer a new view of thunderstorm electrification which is complementary to the view provided by satellite optical imagers [*Boccippio et al.*, 2000; *Boccippio et al.*, 1999; *Christian et al.*, 1999a; *Christian et al.*, 1999b; *Light et al.*, 2001; *Suszcynsky et al.*, 2000b; *Suszcynsky et al.*, 2000c].

Because of their possible utility for remotely monitoring thunderstorm processes, we would like to determine how these strong RF pulses relate to the usual unit of thunderstorm activity, which is the “flash”. A flash is a series of sequential signals from a progressing or recurring atmospheric electrical breakdown, usually lasting less than ~ 1 sec and usually involving either progressive development of an ionized channel, or rapidly repeated large-scale currents on the same channel. Flashes are the basic unit to describe lightning occurrence, and a given storm’s flash rate is often a correlate of severe convective weather [*Williams*, 2001]. Flashes can be identified in low-frequency electromagnetic, RF, and optical signals from lightning.

This article uses RF and optical data from the FORTE satellite [*Jacobson et al.*, 1999] to determine statistically the relationship of strong IC radio pulses to flashes. We build on recent case studies [*Jacobson*, 2003; *Jacobson and Light*, 2003; *Light and Jacobson*, 2003] and establish a statistical confirmation of several ideas initially offered in those studies. We will show that the strong RF pulses observed by FORTE are likely to arise from an electrical air-breakdown process that must differ fundamentally from the progressive leader discharge usually invoked to allow air breakdown in sub-threshold electric fields. It will be speculated at the end that a cosmic-ray-instigated breakdown theory [*Gurevich et al.*, 1999] might have relevance to our recent findings on strong RF pulse characteristics and on their relationship to flashes, insofar as the predictions of that model are clear at this time. This speculation is offered in order to instigate more work on these enigmatic radio emissions, rather than to label the cosmic ray model as the unique valid explanation at this early phase in our understanding.

2. FORTE data used in this study

The FORTE satellite carries an RF payload that receives, digitizes, stores, and downlinks discrete records of Very High Frequency (30-300 MHz; VHF) lightning time-series waveforms of the RF electric field, E . The RF receiver whose data are used in much of this study comprises dual, simultaneous 50-Megasample-per-second passbands that are simultaneously digitized, after each is analog-filtered to 22-MHz bandwidth. In the data to follow, we always operated the RF payload with at least one of the 22-MHz-bandwidth channels placed in the range 26-48 MHz, with a nominal 38-MHz center (“low band”). During some of the study, the other 22-MHz-bandwidth channel was tuned to “high band” (118-140 MHz), with a nominal 130-MHz center. Otherwise, the other 22-MHz channel was tuned to low band also, so that both channels were on low-band, but on orthogonal antennas. The trigger for both channels was common and was always derived from the low band. The performance of the FORTE RF payload, plus some of the initial characteristics of the lightning observations, have been described in detail elsewhere [Jacobson *et al.*, 1999]. All data for the present study are from the FORTE low band.

From its launch in August 1997 through December 1999, FORTE operated in a consistent data-taking mode and gathered over 3-million RF records of lightning with the 22-MHz-bandwidth receiver channels. This data will be used in the present study. Details on the data-taking mode during 1997-1999, and on the characteristics of that period’s RF data, have been presented elsewhere [Jacobson, 2003; Jacobson and Light, 2003; Jacobson and Shao, 2002a]. RF signals from intracloud discharges are recognizable by the presence of a time-delayed ground-reflection echo [Jacobson *et al.*, 1999]. By contrast, RF signals associated with near-the-ground discharge processes lack a time-resolved ground echo [Jacobson and Shao, 2002a]. The present study will include only intracloud-discharge signals and will exclude all RF signals lacking a recognizable ground-reflection echo. Thus, we will consider only those intracloud-discharge RF pulses that are sufficiently narrow ($<10 \mu\text{s}$) to allow clear resolution of the range of time delays (10-150 μs) associated with the delayed echo. In this manner we can deduce the discharge height for each pulse whose origin’s latitude and longitude are known [Jacobson *et al.*, 2000; Jacobson *et al.*, 1999].

For the case of narrow RF pulses having clear ground-reflection echoes, it has been shown [Jacobson and Light, 2003] that these pulses tend to belong to one of two general classes. The first class (“strong pulses”) are the brightest RF signals recorded by FORTE. They have somewhat extended width (typically 2-4 μs), have random amplitude variations within the pulse at sub-microsecond timescales, and usually have a several-microsecond coda of weak emission extending after the main pulse. The strong pulses have been shown sometimes, but not always, to be associated with NBEs [Smith *et al.*, 1999]. The second class (“coherent pulses”), by contrast, are two to three orders-of-magnitude weaker, are narrow (on the order of 0.1 μs when suitably measured), are coherent (that is, they consist of a simple pulse with no random amplitude variations versus either time or frequency within the pulse), and are perfectly linearly polarized. These coherent/polarized pulses are associated with steps in a progressive leader breakdown [Jacobson, 2003; Jacobson and Light, 2003].

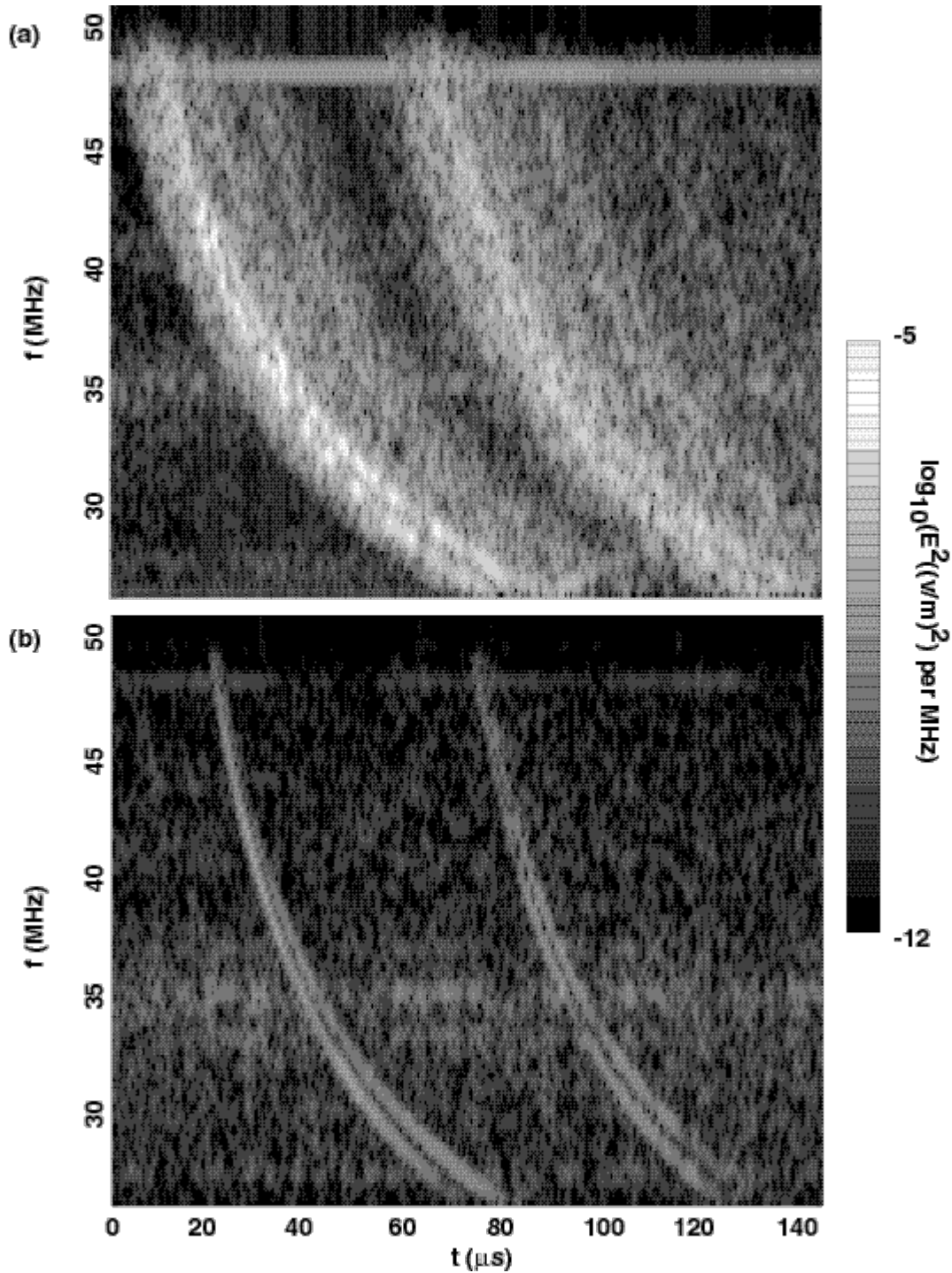


Figure 1: Spectrograms of (a) strong intracloud pulse, and (b) polarized/coherent intracloud pulse. The ground echo is seen at a delay of $\sim 50\text{-}60 \mu\text{s}$ relative to the main pulse in each case. The spectrogram is computed with a sliding short-period Fourier transform having $\sim 1\text{-}\mu\text{s}$ width. Grey-scale key is shown at right and is common to the two examples.

Figure 1 [after *Jacobson and Light, 2003*] shows examples of the two classes of pulses in moving-window-spectrogram form. The top signal (Figure 1a) is from the strong-pulse class. The bottom signal (Figure 1b) is from the coherent/polarized-pulse class. The logarithm of the spectral density is coded in grey-scale; the same scale is common to both signals. The spectrograms' sliding Fourier window is about 1 μ s wide, so the coherent/polarized pulse's 0.1- μ s intrinsic width is artificially broadened by the Fourier windowing in Figure 1. The strong pulse shows extended width compared to the coherent/polarized pulse. The strong pulse also shows a low-power coda that is lacking in the coherent/polarized pulse. Finally, the strong pulse has irregularly varying spectral amplitude but is much more intense overall, compared to the coherent/polarized pulse. In addition to lightning in these signals, there is some interference (horizontal bands) from anthropogenic narrow-bandwidth radio transmissions. In each spectrogram, the ground-reflection echo is delayed $\sim 50 \mu$ s from the primary pulse. This implies that the echo has propagated $\sim 50 \mu$ s/c ~ 17 km further than the primary pulse. If the satellite were at zenith relative to the lightning, this would imply a height above ground of ~ 8.5 km. This height is a lower estimate; if the satellite is not at zenith, the implied RF-emission height must be greater [*Jacobson et al., 1999*]. Each signal exhibits obvious spectral dispersion from ionospheric propagation [*Jacobson et al., 1999; Roussel-Dupré et al., 2001*], with most of the group delay due varying as $\sim \text{TEC}/f^2$, where TEC is total electron content, that is, the path integral of the electron density along the line-of-sight, and where f is the radio frequency. (The TEC is inferred to be $5.36 \times 10^{17} \text{ m}^{-2}$ in Figure 1a and $3.43 \times 10^{17} \text{ m}^{-2}$ in Figure 1b, using the automatic data reduction described elsewhere [*Jacobson et al., 1999*]). In addition, each signal shows pulse splitting at finer time-scales due to ionospheric birefringence in the geomagnetic field [*Jacobson and Shao, 2001; Massey et al., 1998*].

3. Flashes versus isolated discharges

FORTE is visible to a given storm for typically 100-500 s, during which FORTE might record from just a few, to hundreds, of signals from that storm. The overall duration of the FORTE visibility, divided into the number of signals that are recorded, gives the random rate of triggers from that storm. Sometimes the triggers indeed appear to occur at random times, with little clustering into groups. For other storms, the FORTE-recorded events occur in clusters that correspond to the several recurrent steps of an IC "flash", or temporally-clustered group of IC discharge steps that emit detectable RF radiation. We will develop a quantitative measure of this difference in order to highlight certain key properties of strong-pulse events and of those events' relationship to other lightning processes.

Figure 2 shows the square of the recorded low-band peak RF electric field (Figure 2a), and the line-of-sight TEC (Figure 2b), during FORTE's pass near a storm. The values of E^2 span three orders-of-magnitude in this storm. Let us divide events according to four subranges of $\log_{10}(E^2 ((\text{v/m})^2))$. For each of these subranges, Figure 3 shows the probability that any given event (considered as a key event) from this storm will have neighbors in a time differential relative to the key event. The key event is associated with

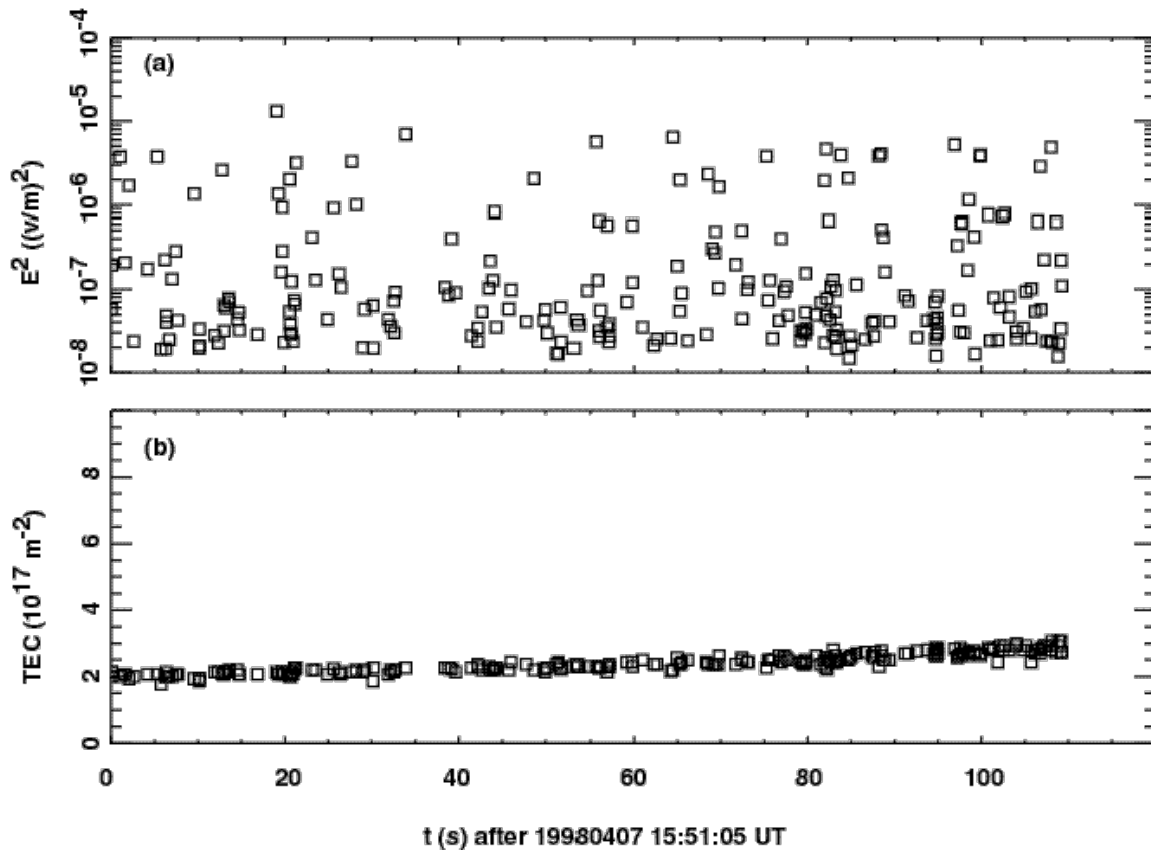


Figure 2: (a) Square of received electric field in the FORTE low band (26-48 MHz), and (b) TEC versus time, during a FORTE pass in view of a storm producing RF pulses recorded by FORTE. As for this entire study, only IC pulses meeting pulse-quality criteria (see text) are included.

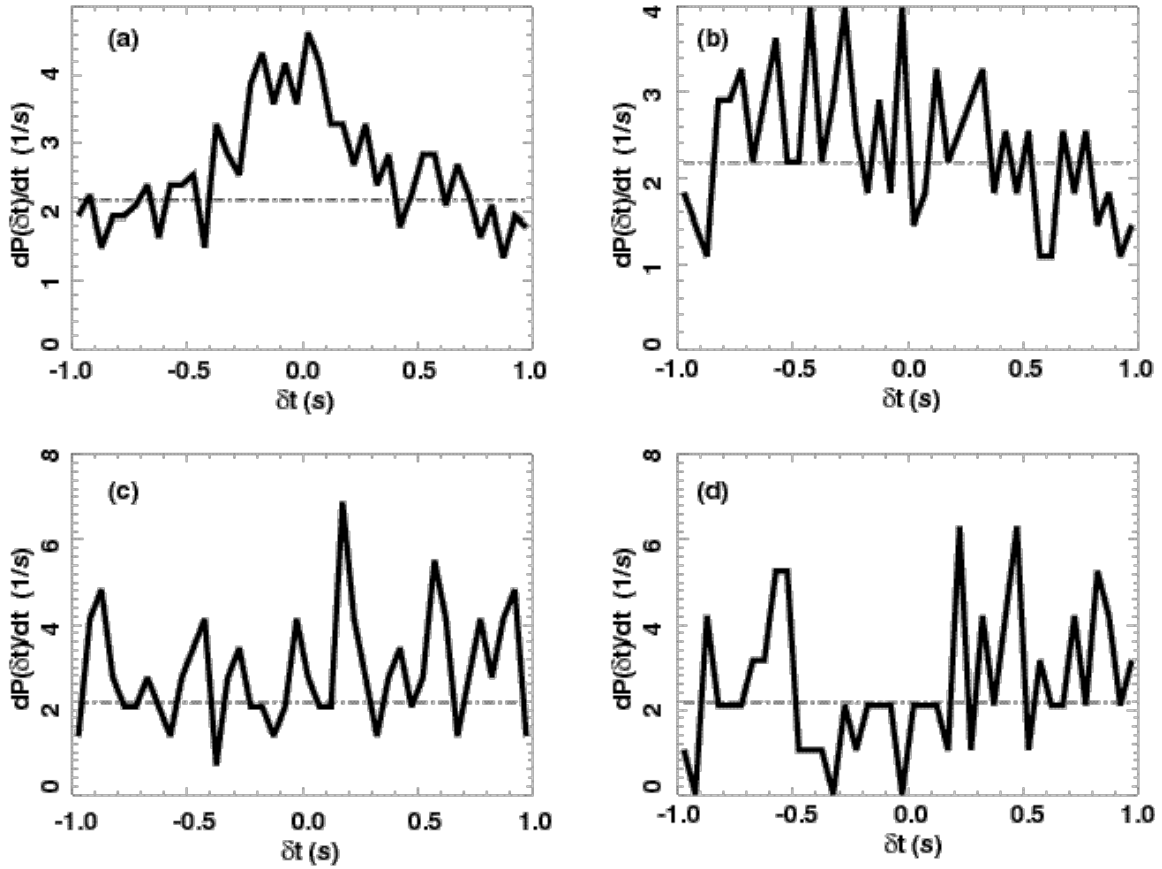


Figure 3: Probability of neighbor events per unit time, versus offset of neighbor time relative to key-event time. Each key event is within one of four selected E^2 subranges, while the neighbor events can be of any E^2 . The four subranges of $\log_{10}(E^2 ((v/m)^2))$ are (a) -7.83 to -7.09 , (b) -7.09 to -6.35 , (c) -6.35 to -5.62 , and (d) -5.62 to -4.88 . The dot-dash horizontal line in each plot is the expected random rate of triggers based on the overall duration and number of events in the visibility pass.

the selected E^2 subrange, while the neighbor events can be of any E^2 . The four subranges of key-event $\log_{10}(E^2 \text{ ((v/m)}^2))$ are (a) -7.83 to -7.09 , (b) -7.09 to -6.35 , (c) -6.35 to -5.62 , and (d) -5.62 to -4.88 . The dot-dash horizontal line in each plot is the expected random rate of triggers based on the overall duration and number of events in the visibility pass. There is a very slight surplus of neighbors, relative to the random rate, for key events in the lowest class of E^2 , and essentially no surplus in the three other key-event classes of E^2 . Figure 3 shows that the storm's RF emissions recorded by FORTE are mainly isolated from each other; that is, their clustering into flashes is hardly enhanced over the rate from random occurrence within the storm pass.

By contrast, Figure 4 shows the square of the recorded low-band peak RF electric field (Figure 4a), and the line-of-sight TEC (Figure 4b), during FORTE's pass near a storm in which all the 127 FORTE-detected RF records are tightly clustered into five high-occupancy flashes. Each flash has a distinct high-intensity pulse and many more pulses at orders-of-magnitude lower intensity. Again, we divide events according to the storm's own four subranges of $\log_{10}(E^2 \text{ ((v/m)}^2))$. Figure 5 is like Figure 3 but for the flash-dominated storm introduced in Figure 4. For this second storm, the four subranges of $\log_{10}(E^2 \text{ ((v/m)}^2))$ are (a) -8.1 to -7.4 , (b) -7.4 to -6.7 , (c) -6.7 to -6.0 , and (d) -6.0 to -5.28 . Again, as in Figure 3 above, Figure 5 shows the probability of any given event (considered as a key event) having neighbors in a time differential relative to the key event. The key event is associated with the selected E^2 subrange, while the neighbor events can be of any E^2 . The dot-dash horizontal line again shows the random expectation of neighbors. This random level is now very small compared to the flash peaks in all four classes of key-event E^2 . This is because the second storm has pulses that are highly clustered into discrete, high-occupancy flashes. Another feature evident from Figure 5 is that the more intense key events tend to precede their neighbor events in the same flash, as noted elsewhere [Jacobson, 2003; Jacobson and Light, 2003]. Whereas the neighbor-event timing distribution is almost symmetric in the less-intense categories of key events (Figure 5a and 5b), the distribution is entirely skewed to retarded times in the more-intense categories of key events (Figure 5c and 5d).

Figures 3 and 5 suggest a simple statistic for characterizing the "flashiness" of storms: We shall evaluate the random expectation of flash neighbors in the relative-time range ± 50 millisecond for any given storm pass by FORTE, and divide this random rate into the actual number of neighbors observed in the relative-time range ± 50 millisecond, using all events as key events in developing the statistic. This statistic will be called "flash-enhancement factor", or FEF. The case of purely random neighbors (i.e., isolated events with no evidence of grouping into flashes) will be indicated by $FEF \sim 1$. For example, the case of Figures 2 and 3 has $FEF < 2$. The case of significant grouping into flashes, with long voids in between the flashes, will be indicated by $FEF \gg 1$. For example, the case of Figures 4 and 5 has $FEF > 100$. It is important to note that FEF characterizes a storm, or more precisely the storm as recorded by all the FORTE RF data records for that storm, and is not defined by an individual FORTE RF data record itself.

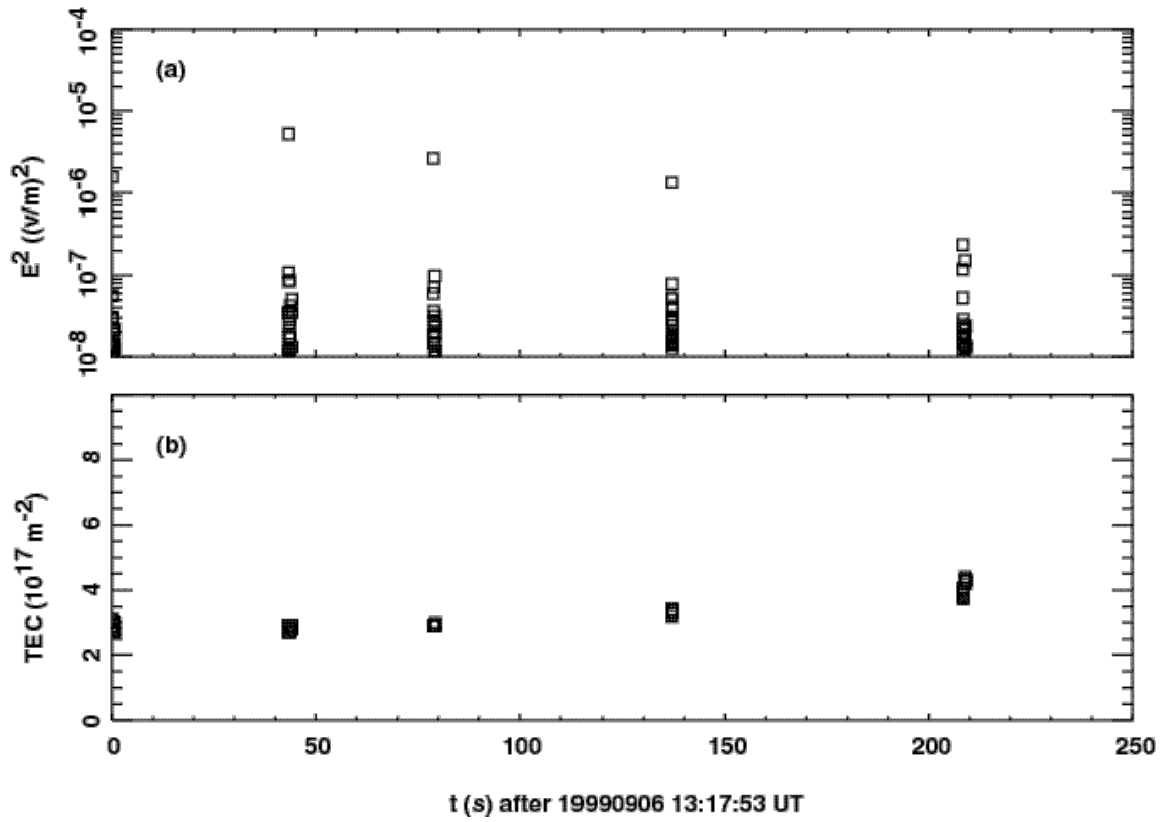


Figure 4: Similar in format to Figure 2, except for a storm with all 127 events concentrated into just 5 flashes.

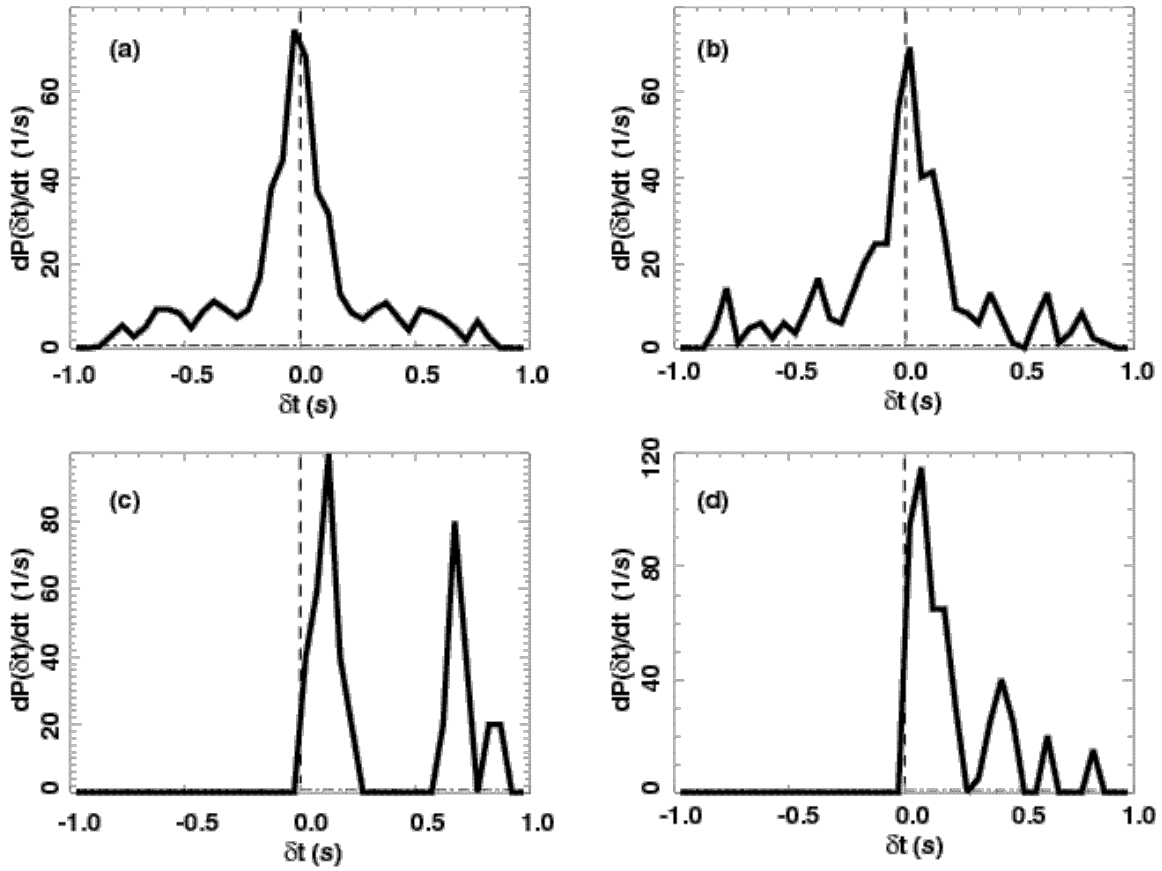


Figure 5: Similar in format to Figure 3, except for the storm of Figure 4 and containing five flashes. The four subranges of $\log_{10}(E^2 \text{ (v/m)}^2)$ are (a) -8.1 to -7.4 , (b) -7.4 to -6.7 , (c) -6.7 to -6.0 , and (d) -6.0 to -5.28 .

4. Study of FORTE data with geolocated sources

4.1 Methods of geolocation

The FORTE 1998-9 archive of RF data has been used to identify a total of 4603 storm passes that are relatively isolated, so that the data in each pass can be confidently attributed to one storm and not to an overlay of more than one storm. These 4603 storms contain 386,444 IC pulses overall meeting the standard quality criteria. We shall now choose a subset of these 4603 storms.

For IC events whose signal-source horizontal locations (latitude, longitude) are known, we can calculate the RF emission height, which is proportional to the product of (1) the time delay of the ground-reflection echo and (2) a geometrical factor related to the separation of the emission from the subsatellite point [Jacobson *et al.*, 1999]. We can also use the source location to calculate the effective radiated power (ERP) referenced to the source, which is more physically significant than E^2 at the satellite. Henceforth in this paper, “ERP” will imply ERP in the FORTE low band (26-48 MHz).

RF signals recorded by FORTE do not by themselves reveal the signal-source location, other than being in the portion of Earth viewed by FORTE at that instant. However, the horizontal location of sources of RF signals recorded by FORTE is in many cases ascertainable by time-correlation of the RF trigger time with the times of other signals from sensor systems that provide location through either time-difference-of-arrival (TDOA) or imaging approaches. The original work of this type used the low-frequency and very-low-frequency (LF and VLF) National Lightning Detection Network to provide horizontal locations of sources for FORTE RF signals [Jacobson *et al.*, 2000]. Soon thereafter, FORTE RF signal sources were successfully located by time correlation with signals from FORTE’s own Lightning Location System (LLS) [Light *et al.*, 2001; Suszcynsky *et al.*, 2000b]. That instrument is based on NASA’s OTD and LIS instruments [Christian *et al.*, 1999b]. We have also studied locations for RF signals via joint correlation with both LLS and PDD, the “Photodiode Detector” on FORTE [Kirkland *et al.*, 2001]. This triple-coincidence requirement provides a smaller but more reliable geolocation set than does coincidence with LLS alone, as the PDD, unlike the LLS, is insensitive to energetic particles. Finally, some FORTE signal sources have been identified by correlation with two other LF/VLF arrays using TDOA to infer location: The “Edot array” [Heavner *et al.*, 2002; Smith *et al.*, 2002] based largely in Florida but with some coverage of the New Mexico region, and the United Kingdom Meteorological Office (UKMet) array of VLF DTOA detectors [Lee, 1986].

The distribution of ERP in FORTE’s geolocated RF events is partly biased by our methods of geolocation. This is not only a limitation, though, but also a source of insight. Figure 6 shows the distribution of $\log_{10}(\text{ERP}(W))$ with a bin size of 0.2, for each of five geolocation methods. Each curve has been separately normalized for easy comparison. The curve in Figure 6 labeled “LLS” refers to the LLS imager, and the curve labeled “PDD/LLS” refers to a further requirement that not only the LLS imager but also FORTE’s PDD photometer be in temporal coincidence with the RF record. Otherwise,

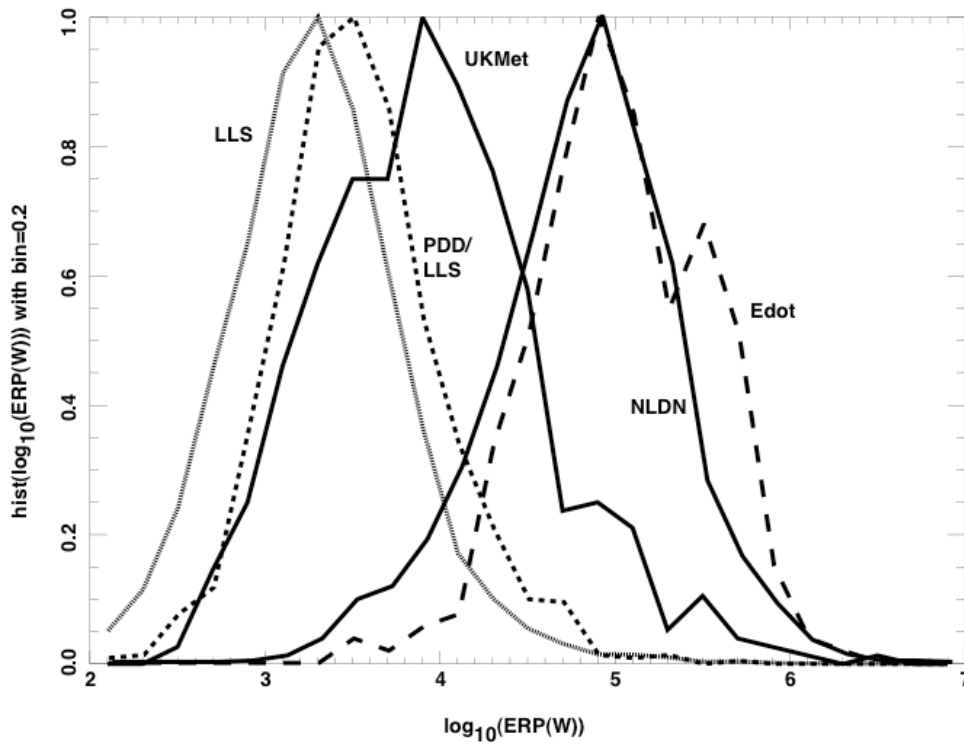


Figure 6: Relative histograms of $\log_{10}(\text{ERP}(W))$ for those intracloud RF events that are directly geolocated via time-coincidence with other detection systems. The passband is the FORTE low-band, 26-48 MHz. The source of geolocation is marked as FORTE's Lightning Location System (LLS), LLS plus FORTE's Photo Diode Detector (PDD), the United Kingdom Meteorological Office TDOA array (UKMet), the National Lightning Detection Network (NLDN), and Los Alamos spheric-waveform array (Edot). The binsize is 0.2.

both LLS and PDD/LLS are alike, in that the RF event is accompanied by a detectable optical event. Both optical-concurrence curves are biased toward low RF ERP. Besides the two curves for optical concurrence, all three other curves in Figure 6 are for RF events located through concurrence with LF/VLF TDOA sensor arrays. All of these classes of RF events have higher-ERP distributions than do the optically-concurrent events. The Edot-concurrent events have slightly higher ERP than do the NLDN-concurrent events, while the UKMet-concurrent events are shifted to weaker ERP relative to either the Edot- or NLDN-concurrent distributions.

4.2 Borrowed geolocations for entire storms

Of the FORTE RF pulses whose source locations have been directly determined by correlation with other systems, many of these pulses can be clearly associated with other FORTE RF pulses, either in the same flash or in at least the same storm. It is then possible for the clearly associated pulses to “borrow” the source location of a pulse whose source is known. In this manner we can calculate both an IC-discharge height and an at-source ERP *for every event in the storm*. This borrowing procedure has been described in detail elsewhere [Jacobson, 2003; Tierney *et al.*, 2001]. Using this borrowing procedure, as well as standard pulse-quality selection criteria [Jacobson, 2003] we arrive at a total of 71,323 quality RF records of pulsed IC signals for which we can reliably know the source horizontal location and which lie in storms containing at least 20 events. (We disregard storms containing fewer than 20 events.) These RF signals are distributed amongst 636 different storms surviving this selection, for an average of about 110 recorded events per geolocated storm. These 71,323 events and their 636 storms provide the data for the rest of this study. Each of these 636 storms is characterized with an FEF parameter determined for that storm.

4.3 ERP-dependent flash characteristics

Figure 7 shows the 71,323 events’ distribution of $\log_{10}(\text{ERP}(W))$ in the FORTE low band (26-48 MHz), with a bin size of 0.1, over a five-decade range of ERP. We divide this ERP range into four classes as shown by the vertical dashed lines: (a) ERP = 100 W to 2 kW, (b) ERP = 2 kW to 5 kW, (c) ERP = 5 kW to 40 kW, and (d) ERP = 40 kW to 10 MW. These ERP classes will now be used to determine ERP-dependent trends in other characteristics of the RF pulses.

The flash-enhancement factor (FEF), introduced above in Section 3, characterizes the degree of temporal association of different recorded RF signal records from the same storm. Figure 8 shows the probability distribution of FEF for each of the four ERP classes (introduced above in Figure 7). The distribution uses all 71,323 selected IC signals, split into the ERP classes. Of course there are only 636 independent storms and hence only 636 independent values of FEF. The distribution is of the FEF for the IC signal’s parent storm, since FEF characterizes a storm and not a single record. The left-most bin is for FEF in the range 0 to 5. Storm passes with such a low FEF parameter consist of quasi-isolated, randomly timed pulses, typified by the storm illustrated in Figures 2 and 3 above. We see from Figure 8 that over 55% of RF records in the highest-ERP class (d) have FEF <5, while the percentage in this class steadily declines for lower-ERP (c, b, and a in order of decreasing ERP) classes. Overall, Figure 8 shows that the highest-ERP IC

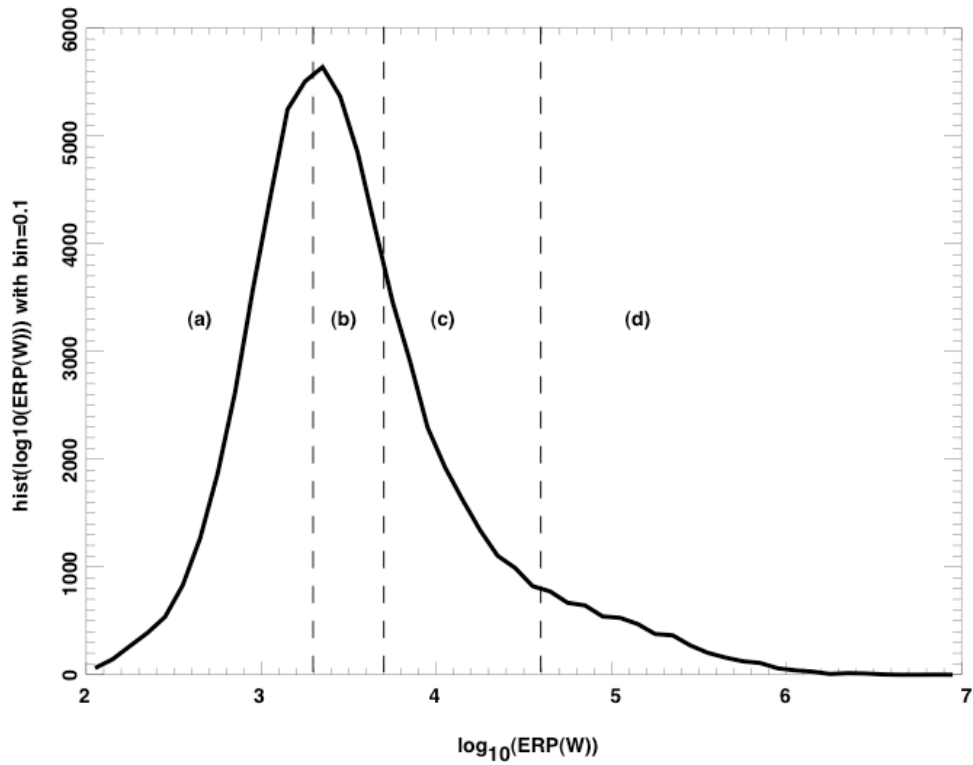


Figure 7: Histogram of $\log_{10}(\text{ERP}(W))$ for all 71,323 IC RF pulses. These events are from 636 storms that are geolocated. The binsize is 0.1. The four defined ranges of ERP (a through d) are separated by vertical dashed lines.

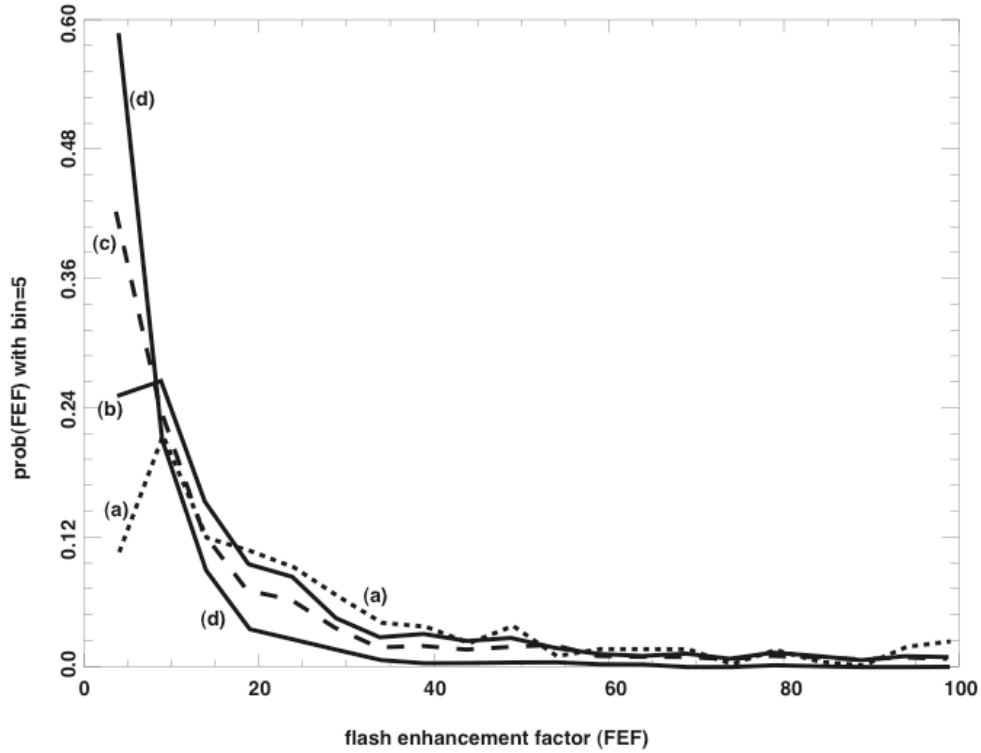


Figure 8: Parent-storm flash-enhancement factor FEF, defined as the factor by which the number of neighbor events in ± 50 millisecc exceeds the number expected if the events were randomly placed within the storm pass. The FEF is computed for each storm. The four curves are for the four defined ranges of key-event ERP: (a) ERP = 100 W to 2 kW, (b) ERP = 2 kW to 5 kW, (c) ERP = 5 kW to 40 kW, and (d) ERP = 40 kW to 10 MW; see Figure 7 above.

records tend to occur in storms that have less concentrated flashes and more isolated emissions, while the lowest-ERP records tend to occur relatively more often in storms with concentrated flashes. This is consistent with the original finding on Narrow Bipolar Events [Smith *et al.*, 1999], that NBEs tended to be isolated in time. The present observations with FORTE permit us to look with high dynamic range and to observe some flashes with which high-ERP signals are associated, however. This is responsible for the high-FEF extension of curve (d) in Figure 8.

We now examine intraflash characteristics as a function of event ERP. To do this we need to restrict our attention to storms having flashes, not just (or even primarily) isolated RF emissions. The next three figures in this section are thus further restricted to storms having at least a moderate concentration of the recorded events into flashes: FEF>10. This cuts the pool of qualifying events from 71,323 down to 35,429, and cuts the pool of parent storms from 636 down to 294.

The most basic trend controlled by ERP is the number and relative timing of neighbor events. Figure 9 shows the probable number of neighbor events in a 50-millisecond-wide bin versus bin delay (=neighbor time minus key-event time). The four ERP classes of key events are labeled as for Figure 7 above. As key-event ERP increases, going from class (a) to class (d), the overall number of neighbors decreases. (Note that curve (d) is scaled upward by a factor of 5 for easy comparison with the others.) For the three lowest-ERP classes of key events (a, b, and c: cumulatively, ERP =100 W to 40 kW), the neighbor events are roughly as likely to precede ($\Delta t < 0$) as to follow ($\Delta t > 0$) a key event. By contrast, for the highest-ERP class of key events (d: ERP = 40 kW to 10 MW), the neighbor events preferentially follow the key event ($\Delta t > 0$). This provides statistical confirmation of previous case studies which found that high-power RF emissions accompany a process serving to initiate certain intracloud flashes but not occurring in the midst of a flash [Jacobson, 2003; Jacobson and Light, 2003; Rison *et al.*, 1999; Thomas *et al.*, 2001].

Another requirement will now be imposed on the definition of flashes for the final two figures of this section: In addition to requiring the parent storm to have FEF > 10, we now furthermore require a valid flash not to have temporal gaps (between flash members) greater than 200 milliseconds. If a gap exceeds 200 milliseconds, then the algorithm terminates one flash and counts a new flash as having begun.

We now examine the emission height of subsequent (i.e., not initial) events within a flash, scaled by the emission height of the initial event of the flash. This ratio indicates whether the subsequent events within a flash have a preferred altitude relationship to the initial event of the flash. Figure 10 shows this ratio for all four classes of initial-event ERP. For initial events in the three lowest-ERP classes (a, b, and c: cumulatively, ERP =100 W to 40 kW), the subsequent events are only slightly more likely to occur above, rather than below, the initial event. However, for initial events in the highest-ERP class (d: ERP = 40 kW to 10 MW), the neighbor events preferentially occur higher in altitude than the initial event. This statistically confirms the case-study examples presented elsewhere [Jacobson, 2003; Jacobson and Light, 2003; Thomas *et al.*, 2001]. The explanation for

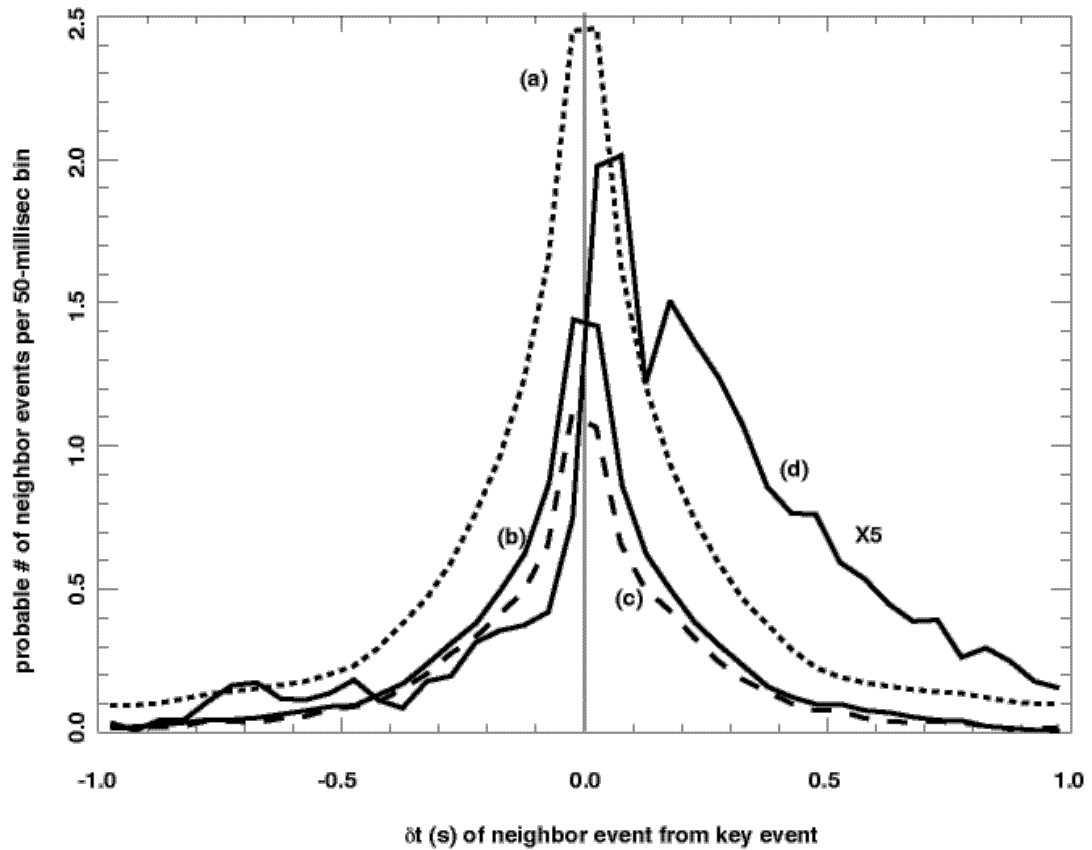


Figure 9: Probable number of neighbors per 50-millisecond bin, versus offset of neighbor time relative to key-event time. The key events lie in four defined ranges of key-event ERP: (a) ERP = 100 W to 2 kW, (b) ERP = 2 kW to 5 kW, (c) ERP = 5 kW to 40 kW, and (d) ERP = 40 kW to 10 MW. Curve (d) has been scaled up by a factor of 5 for easy comparison with the other curves.

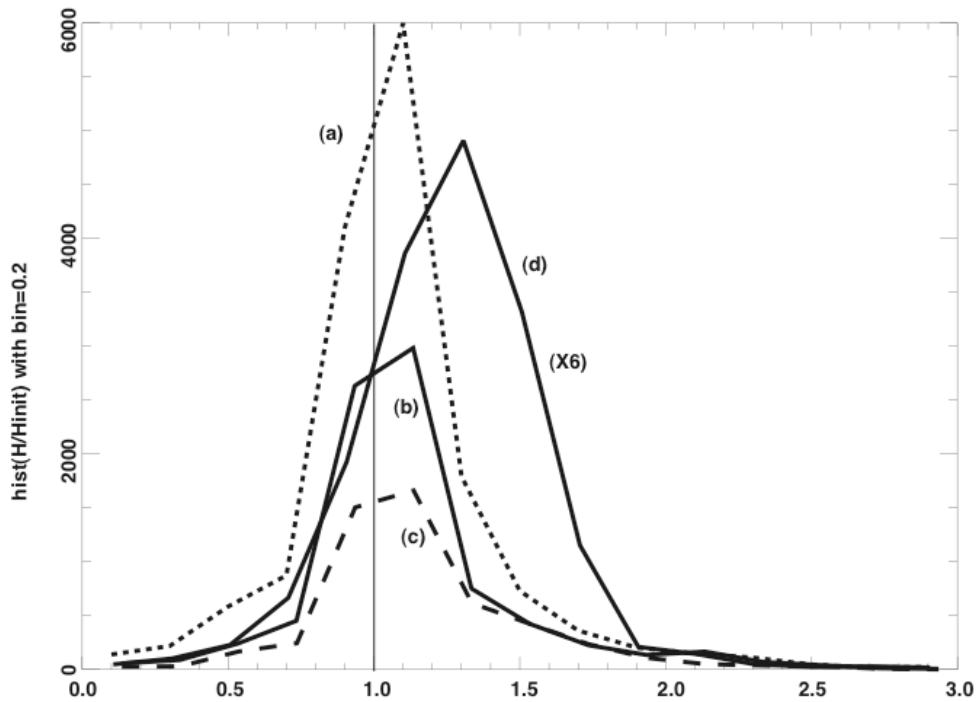


Figure 10: Histogram of subsequent-event height, divided by initial-event height, for flashes with initial event in four ranges of initial-event ERP: (a) ERP = 100 W to 2 kW, (b) ERP = 2 kW to 5 kW, (c) ERP = 5 kW to 40 kW, and (d) ERP = 40 kW to 10 MW. Curve (d) has been scaled up by a factor of 6 for easy comparison with the other curves. Flashes are included only for parent-storm FEF > 10.

this may be that the energetic initiator event occurs in the high electric field between an underlying negative charge layer and an overlying positive charge layer, and that the subsequent lower-power events are part of a negative leader progressing within the positive charge layer [Thomas *et al.*, 2001].

As noted earlier in connection with Figure 1, the strong RF pulses are broader (typically 2-4 μ s) than are the coherent/polarized pulses. The latter's width is on the order of 100 ns when appropriately determined [Jacobson and Light, 2003], but is instrumentally broadened to \sim 1.4 μ s when determined robotically for the FORTE RF database generator. Figure 11 shows the ratio of the pulsewidth in subsequent events within a flash to the pulsewidth of that flash's initial event, for each of the four classes of initial-event ERP. The highest-ERP class (d: ERP = 40 kW to 10 MW) of initial events are usually followed by subsequent events that tend to be less wide, by a factor typically of 1/2. This is consistent with the previous findings that the highest-ERP events are wider pulses (Figure 1) and that they mostly initiate, but do not occur later within, flashes with which they are associated (Figure 9).

5. Relationship of strong RF events to Narrow Bipolar Events

5.1 Background

Some of the earliest observations on Narrow Bipolar events [Le Vine, 1980] used simultaneous recording at VHF and Very Low/Low/Medium Frequency (VLF/LF/MF). The VHF signal in Le Vine's ground-based recordings corresponds to FORTE's RF signal, while the VLF/LF/MF "field change" signals in Le Vine's ground-based recordings correspond to today's Edot array signals [Smith *et al.*, 2002]. Comparing the RF and field-change amplitudes for the same discharge events, Le Vine stated "There was no apparent correlation between the strength of the RF radiation and the size of the associated field change." Later, Willett *et al* [1989] showed evidence that the RF signal is not just a higher-frequency manifestation of the NBE field-change process. Rather, their Figure 2 indicates that the RF signal is an additive noise superimposed upon the slower field-change waveform. Thus it is not surprising that earlier observations revealed no proportionality between RF and field-change amplitudes; there appear to be two processes at work.

The Edot array [Smith *et al.*, 2002] routinely detects and locates, and also is used to infer the peak current, charge-moment change, and (in many cases) the emission heights of NBEs. Figure 12 shows typical waveforms for the electric-field change (high-pass-filtered with a 1-millisecond time constant) for (a) a positive NBE, (b) a negative NBE, and (c) a non-NBE lightning transient for comparison. The data is digitized at 1 Megasample/s after being analog-low-pass-filtered at the Nyquist frequency (0.5 MHz), so Edot recordings do not provide any information on the higher frequencies (RF) that have been observed by other ground-based observations. The two NBEs in Figure 12 are followed first by ionosphere, and second by ground plus ionosphere, reflections of the main pulse. NBEs have been shown to imply large-scale charge-moment changes on the order of tens of Coulomb-km [Smith *et al.*, 1999].

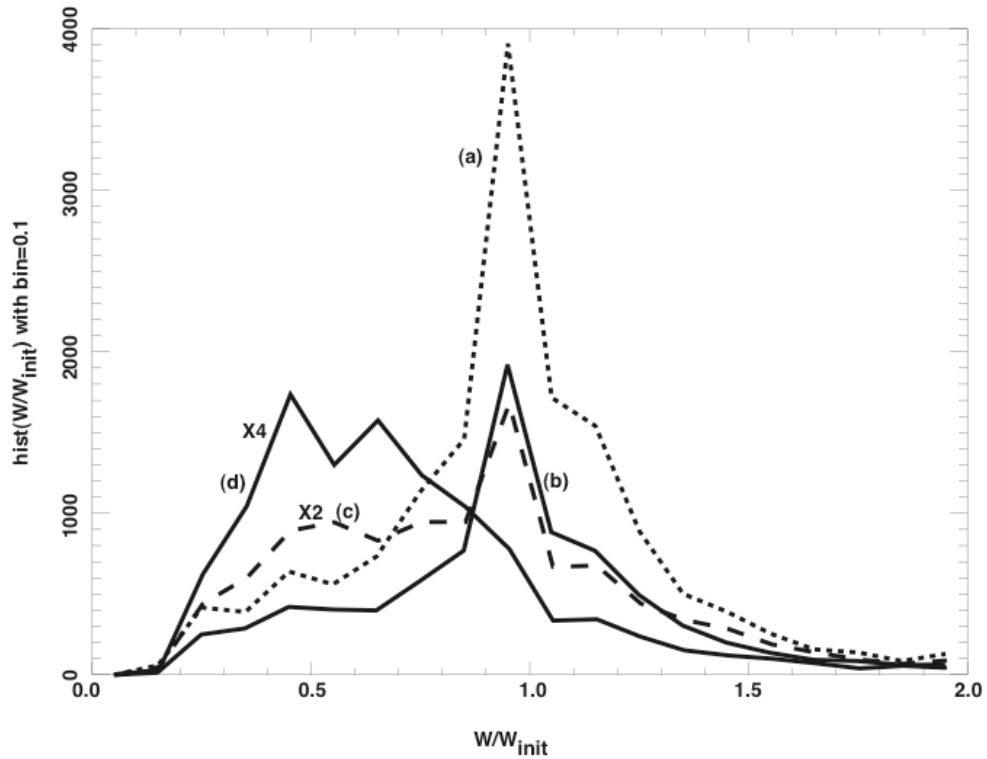


Figure 11: Histogram of subsequent-event pulsewidth, divided by initial-event pulsewidth, for flashes with initial event in four ranges of initial-event ERP: (a) ERP = 100 W to 2 kW, (b) ERP = 2 kW to 5 kW, (c) ERP = 5 kW to 40 kW, and (d) ERP = 40 kW to 10 MW. Curve (c) has been scaled up by a factor of 2, and curve (d) by 4, for easy comparison with the other curves. Flashes are included only for parent-storm FEF > 10.

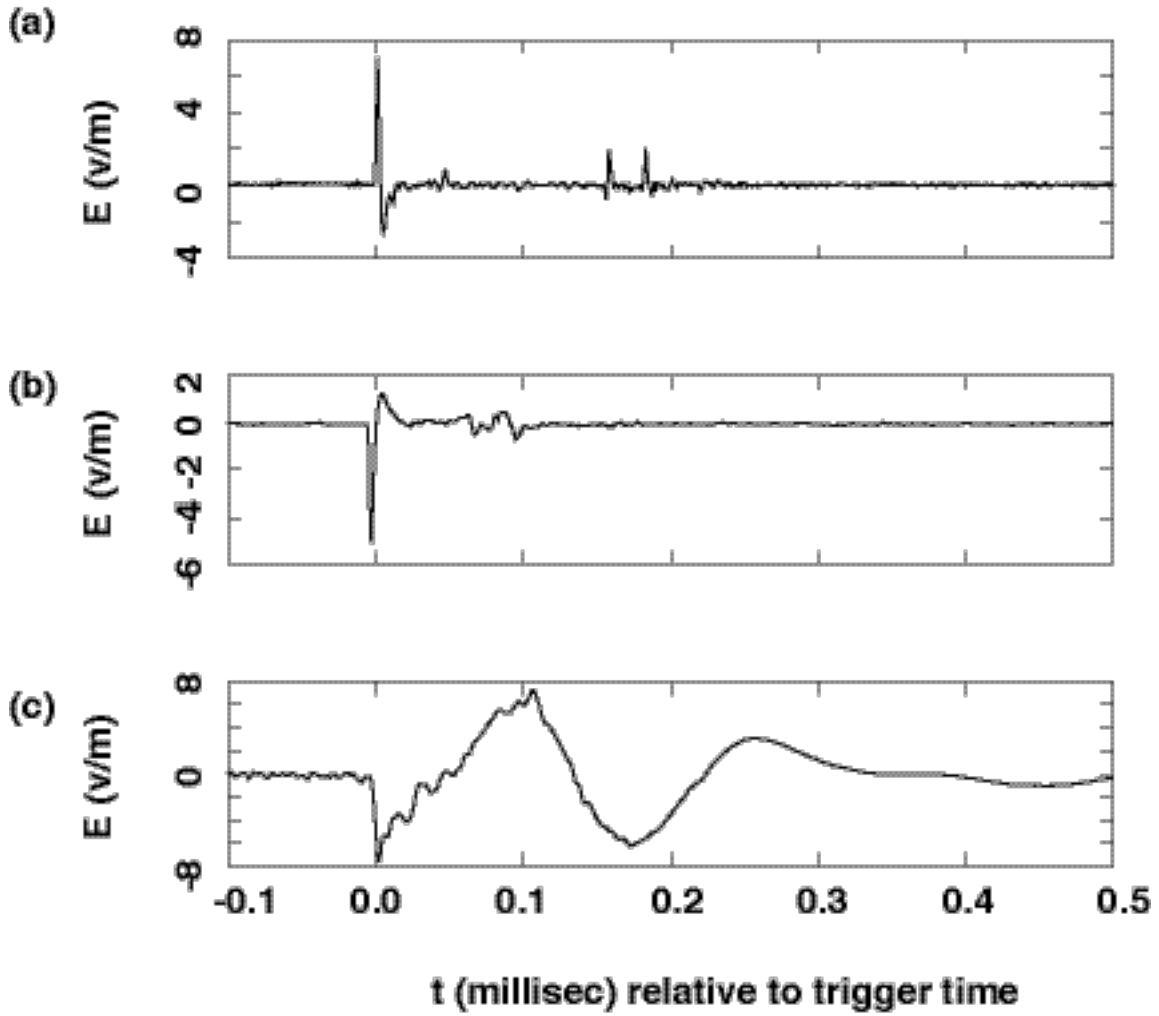


Figure 12: Three waveforms of vertical-electric-field-change signals from the Los Alamos sferic-waveform array (E_{dot}): (a) positive NBE; (b) negative NBE; (c) non-NBE signal. The sensor performs an analog high-pass filtering with time constant ~ 1 millisecond.

5.2 FORTE/Edot common storm observations

Altogether, we have identified 53 FORTE-observed, geolocated storms during 1998-1999 in each of which at least one FORTE event coincides with an Edot NBE. These 53 storms contain a total of 3281 FORTE quality IC pulses. During orbit passes in which FORTE's RF receivers are recording triggered data within view of storms also covered by Edot, there is a possibility of correlating the RF signal (from FORTE) and the field-change signal (from Edot) signals via time coincidence. Figure 13 shows data from a typical joint observation by FORTE and Edot. The format is the same as for Figures 2 and 4 earlier: The TEC is shown in the bottom panel, and the square of the peak pulse electric field, E^2 , is shown in the top panel. Only one of the RF events, circumscribed by a thick diamond symbol, is correlated with an Edot field-change waveform that is an NBE. The storm shown in Figure 13 is quite typical of these 53 storms in two key behaviors:

First, the number of FORTE strong-pulse RF events usually greatly exceeds the number of NBEs; see Section 5.2.1 below.

Second, these storms are always practically devoid of flashes; that is, these storms have low values of FEF; see Section 5.2.2 below.

5.2.1 RF strong pulses without large-scale charge transfer

On the basis of the 53 storms having common Edot and FORTE coverage, and containing at least one FORTE-coincident Edot NBE, we find that *most strong RF events are unaccompanied by Edot NBEs*, and that as a group these unaccompanied RF events are no less intense than are the Edot-accompanied strong RF events from the same storms. The FORTE RF strong pulses that are accompanied by Edot NBEs are a subset of the FORTE RF strong pulses, and are not a higher-ERP subset. We have also checked to ensure that trigger-threshold limitations on the Edot observations are not artificially creating a lack of Edot NBE recordings for the majority of the FORTE strong RF pulses. After performing these checks on our 53 commonly observed storms, we conclude that the majority of FORTE strong RF pulses are simply unaccompanied by large-scale charge transfers. Moreover, the RF pulses lacking large-scale charge transfers are as intense as the minority of pulses that are accompanied by large-scale charge transfers.

We have looked for distinguishing characteristics (e.g. peak ERP, pulse duration, pulse shape, and emission height) which might discriminate a FORTE RF strong pulse which is accompanied by an NBE from another FORTE RF strong pulse in the same storm which is unaccompanied by an NBE. We can find no obvious discriminant in the RF data. Therefore it appears that the RF-emission process is necessary for, but does not require, the completion of the large-scale charge-transfer event giving rise to the NBE. This inference goes a step beyond the implication in the original papers [*Le Vine*, 1980; *Willett et al.*, 1989] that the RF and field-change processes are different. The FORTE/Edot coordinated results imply further that the RF-generating process is necessary for a NBE to be radiated, but that the RF-generating process can occur without an NBE being radiated.

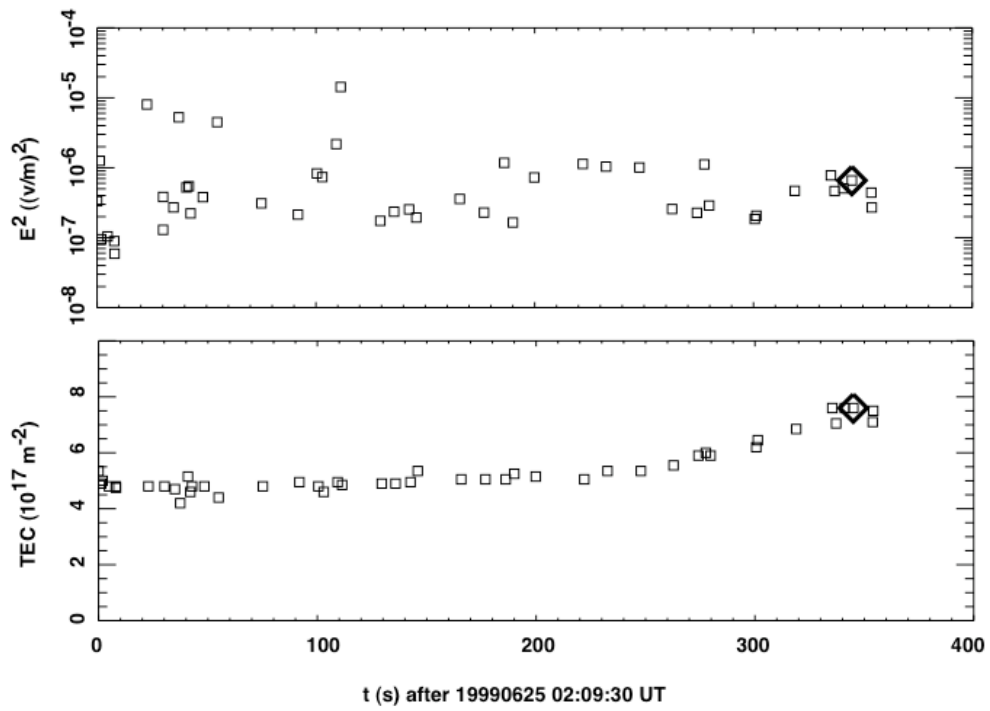


Figure 13: FORTE-observed storm containing one event (marked with a heavy diamond symbol) that is coincident with an NBE observed by Edot. Format same as Figure 2.

5.2.2 Low incidence of flashes in storms containing NBE charge-transfer events

We now compare statistically the likelihood of flashes in the 53 storms having at least one Edot-observed NBE, compared with all 4603 identified storms in the 1998-9 FORTE RF archive. These 4603 identified storms include, but are not limited to, the 636 geolocated storms. The likelihood of flashes is reflected in the FEF parameter. Figure 14 shows the FEF distribution in the 53 NBE-containing storms (dashed curve, after scale-up by factor of (a) 40 and (b) 27) and in all 4603 identified storms (solid curve). The two panels in Figure 14 show (a) the entire FEF range 0-150 and (b) a close-in look at the restricted FEF range 0-30. Both panels show that the NBE-associated storms peak more strongly at the lowest FEF values and achieve almost no high values of FEF, compared to the overall set of identified storms. Statistically *the NBE-associated storms almost never contain flashes*. The FORTE-recorded RF events in these NBE-associated storms tend instead to occur randomly in time and to lack subsequent leader development.

6. Luminous and dark processes within the same flash

Compared with other research satellites observing lightning, FORTE has the unique ability to observe both optical and RF emissions from the same platform. It is interesting to compare the likelihood of optical concurrence as a function of RF pulse strength. Elsewhere it has been shown that IC pulses in the FORTE RF records become more likely to have optical concurrence as E^2 increases, up to a threshold on the order of 10^{-6} (v/m)^2 , above which the optical concurrence rate *decreases* as E^2 increases further [Light and Jacobson, 2003]. This indicates that the RF signals at the highest range of E^2 tend to be generated in a relatively “dark” process, compared to other lightning processes which can trigger FORTE’s optical sensors. Here “dark” is meant not as an absolute but only to indicate that the light output is too weak to trigger FORTE’s optical sensors. That study had the drawback of using emissions that were not geolocated, and thus had to settle for the blurred measure of emission strength afforded by E^2 at the satellite rather than the more relevant measure of ERP at the source. Nonetheless, the finding was new and significant, that the strongest RF IC discharges tend not to have optical concurrence.

The present study uses a smaller dataset, for which however we have the parent storms’ geolocations. In the present study we have already seen (see Figure 6 above) that the RF IC events having direct optical concurrence (“LLS” and “PDD/LLS” in Figure 6) tend also to have the lowest radio powers at the source as measured by ERP. This is not a subtle difference; the ERP of optically-concurrent RF IC pulses is about two orders-of-magnitude weaker than the ERP of Edot-concurrent RF IC pulses. The robustness of this result suggests that the underlying atmospheric process giving rise to high-ERP RF pulses must differ fundamentally from the progressive air-discharge process (leader growth) that gives rise to the low-ERP RF pulses but also to copious light.

In order to test this idea on different processes in the same storm and indeed in common flashes, so that observing biases may be discounted, we have examined by eye several of the storms whose geolocation is by optical concurrence. The optical concurrence preferentially occurs in storms having flashes, that is, having $\text{FEF} \gg 1$. We have seen

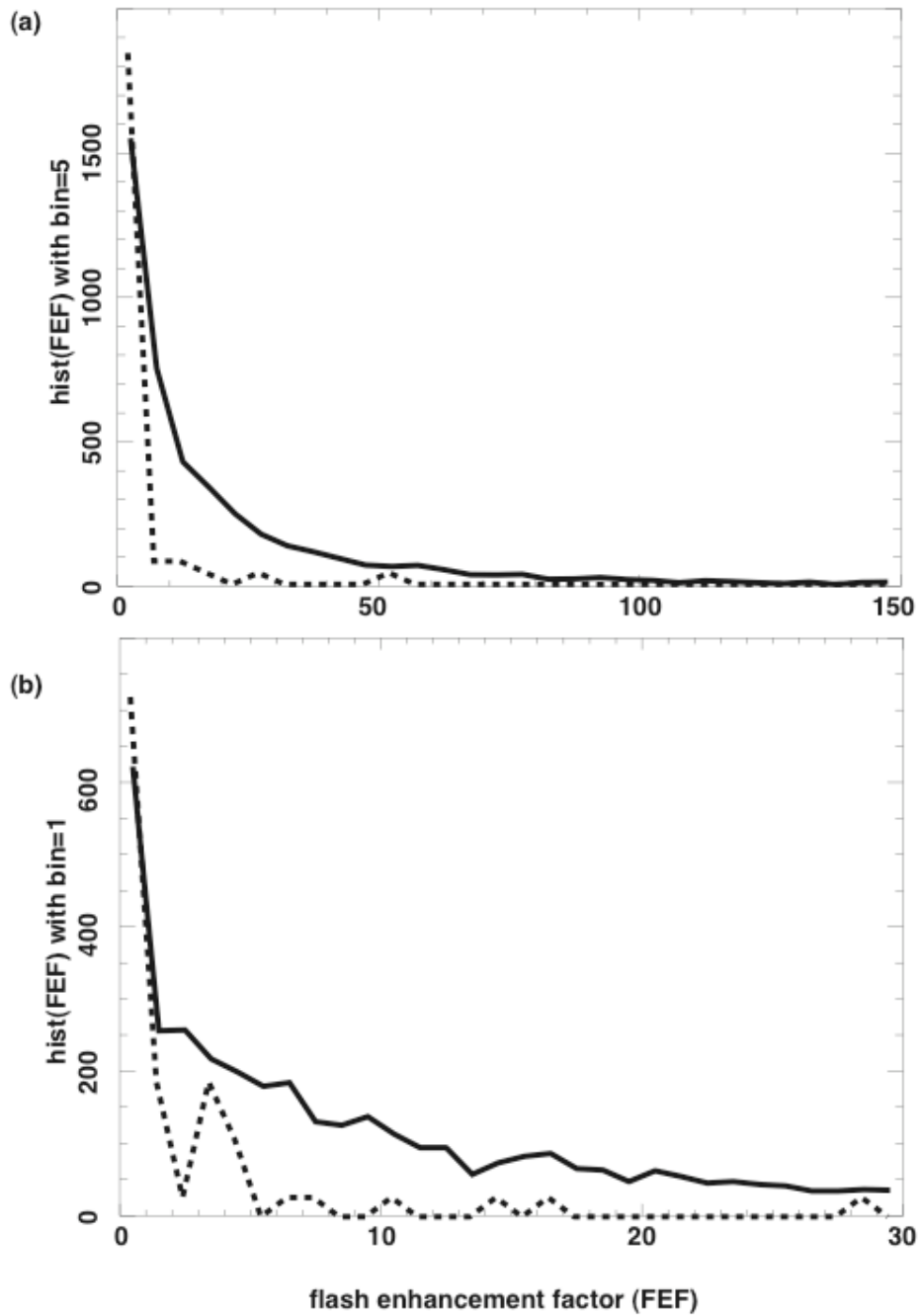


Figure 14: Histogram of flash-enhancement factor FEF for (a) entire FEF range with binsize of 5 and (b) restricted FEF range with binsize of 1. Solid curve is for all 4603 identified storms (not necessarily geolocated storms) in FORTE 1998-9 storm archive, while dashed curve is just for the 53 storms that contain pulses coincident with NBEs observed by Edot. The dashed curve has been scaled up by a factor of (a) 40 and (b) 27 for easy comparison with the solid curve.

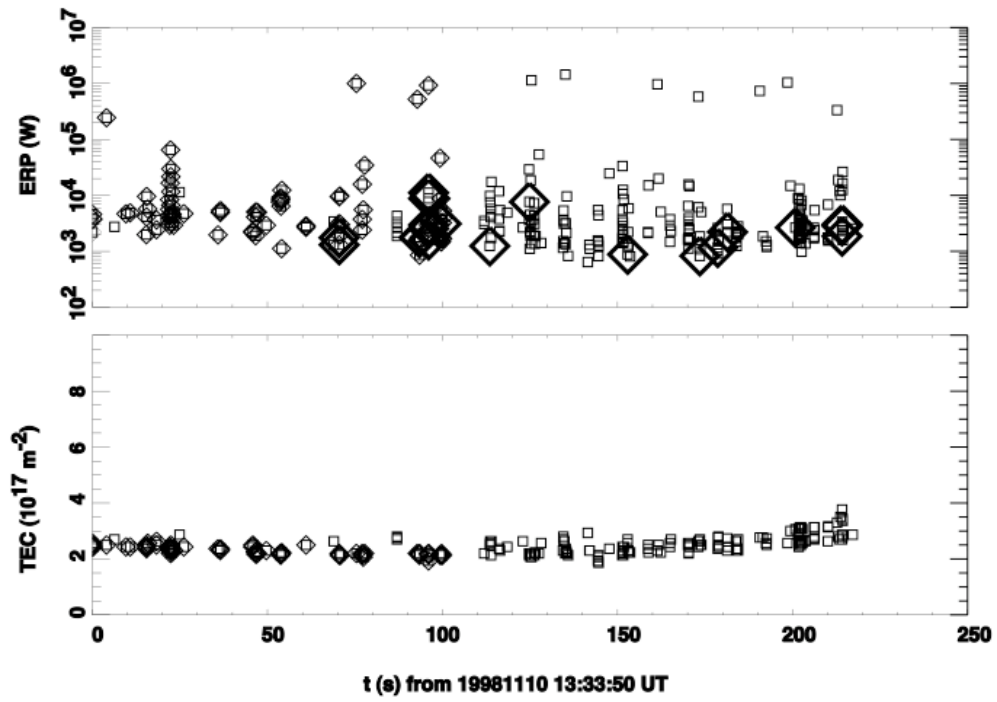


Figure 15: (a) ERP and (b) TEC versus time, for a FORTE pass in view of a storm with LLS-coincident RF events' ERP circumscribed by larger symbols.

very few examples of optical concurrence in storms lacking distinct flashes. This behavior is exactly complementary to the behavior storms whose geolocation is from coincidence with Edot NBEs.

Figure 15 shows a typical optically-geolocated storm pass. The top panel shows ERP, and the bottom panel shows TEC. The storm has distinct flashes, many initiated by megawatt-class pulses. The large, thick symbols circumscribe ERP data points for events having detailed optical concurrence (direct, not just borrowed). The optically-coincident RF signals have two to three orders-of-magnitude less ERP than do the storm's megawatt-class RF pulses. None of the megawatt-class RF pulses have direct optical concurrence. Some of the same flashes in Figure 15 that contain an optically-coincident RF pulse are initiated by an optically-dark, megawatt-class RF pulse. We have examined the optically coincident pulses and confirmed that they are similar to the coherent/polarized pulse shown in Figure 1(b) above.

The transition in optical brightness, between the RF strong and weak pulses in various flashes of Figure 15, can be quantified in terms of a ratio of optical-to-RF outputs. The RF weak pulses in Figure 15 having optical concurrence apparently have a factor of $10^2 - 10^3$ higher optical-to-RF ratio than do the strong pulses. Presumably any differential cloud attenuation of the optical signal from these two pulse types is unlikely to account for this discrepancy in optical/RF ratio. Instead, we infer that the atmospheric processes responsible for the strong and weak RF pulses differ in a physical way from each other, and are not just instances of the same physical process differing in overall amplitude or in cloud attenuation of the optical signal.

7. Limiting amplitude for strong pulses?

The peak-power or ERP distribution of atmospheric RF pulses has been noted in some cases to follow a $(\text{power})^{-1}$ distribution. The Lightning Mapping Array (LMA) [Rison *et al.*, 1999] has observed such distributions on single storms for the bulk of the observed pulses, though the “tail” of exceptionally bright strong pulses, corresponding to FORTE's megawatt-class RF pulses, does not conform to a $(\text{power})^{-1}$ distribution in any particular LMA storm [Thomas *et al.*, 2001]. FORTE does not collect enough pulses in any given storm pass to attempt a meaningful ERP distribution in any given storm, but has been used to assemble a *multi-storm composite* ERP distribution. This distribution also rolls off roughly as $(\text{power})^{-1}$ on the high-power side of the distribution [Jacobson, 2003], where its membership is dominated by the strong IC pulses such as those in Figure 1(a) of the present article. However, in view of the biases introduced by FORTE's reliance on storm geolocation from various supplementary sources (either FORTE optical, or ground-based field-change data), it is questionable whether FORTE's multi-storm composite ERP distribution tells anything useful about the underlying, unbiased ERP distribution of RF pulses.

Evidence from individual storms observed by FORTE suggests instead a truncated rather than a $(\text{power})^{-1}$ distribution. The truncation appears at the high-power end. We have

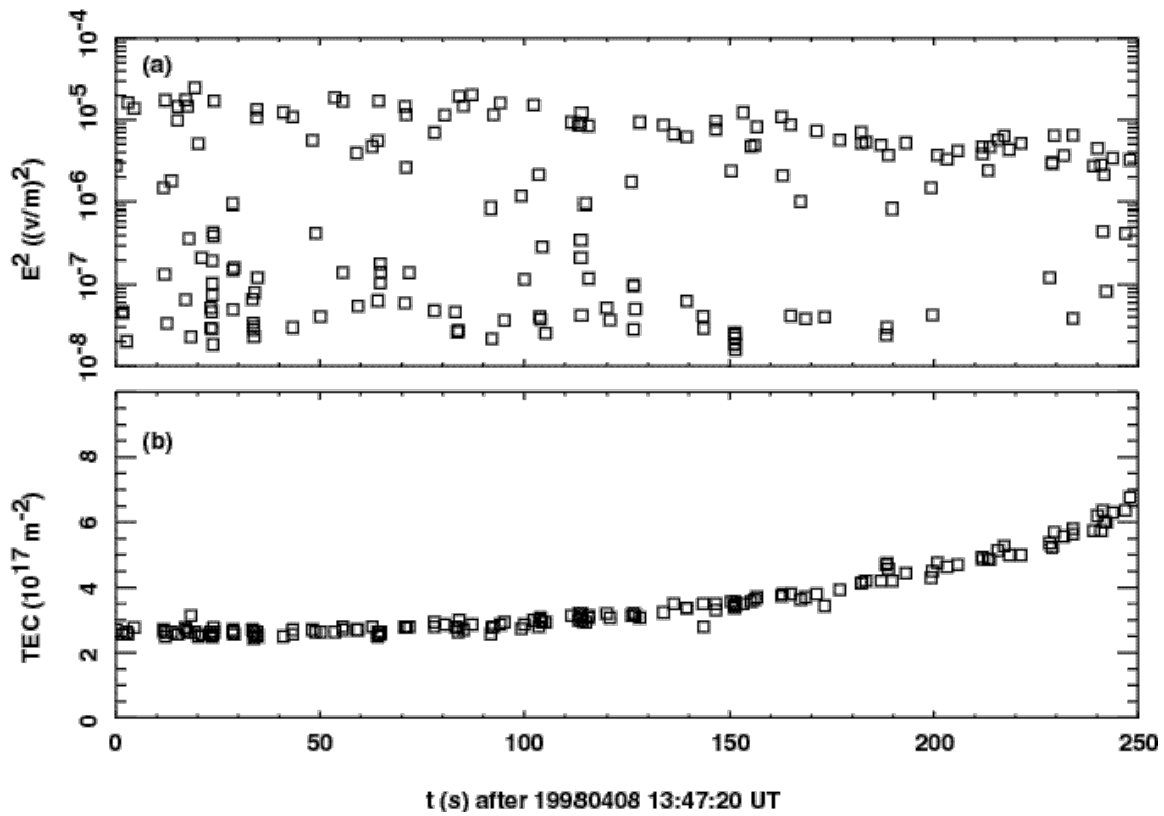


Figure 16: (a) Square of received electric field in the FORTE low band (26-48 MHz) and (b) TEC versus time during a FORTE pass in view of a storm producing RF pulses recorded by FORTE. Illustrates tendency of strong RF pulses to lie below a capping level of E^2 that varies slowly with changing satellite position relative to the storm.

checked on the possibility of FORTE receiver or digitizer saturation as a cause of this truncation, and have found that saturation has never occurred in these geolocated storm observations. The presence of a naturally truncated emission-amplitude distribution can be seen even with storms that are not geolocated, insofar as r^2 varies slowly and smoothly during a FORTE pass in view of a storm, and only r^2 and the smoothly varying antenna lobe [Jacobson and Shao, 2002b] are expected to relate at-satellite E^2 to at-source ERP. For example, Figure 16 shows data on (a) E^2 and (b) TEC in the same format as Figure 2. The slow increase of TEC versus time indicates that the satellite is descending in elevation angle as seen from the source storm, and thus that r^2 is decreasing. The events seem to be truncated at an E^2 top level. The E^2 top level appears also to be slowly descending versus satellite passage. The E^2 top level is remarkably distinct, except for this slow downward trend (presumably controlled by r^2 and the antenna lobe) and a possible oscillation at ~ 70 -s periodicity. The important finding from this example, though, is that there is a clear (albeit slowly varying) capping level of E^2 , above which pulses are not observed. The E^2 capping-level behavior of the storm in Figure 16 is very commonly seen in storms observed by FORTE in which strong RF pulses are present. When we observe such a capping level in ERP for geolocated storms, the level is often at or somewhat above 1 megawatt (referenced to the FORTE low band, 26-48 MHz). The capping level varies somewhat from storm to storm. In any given storm there can be some strong events below the capping level of either ERP or E^2 , but there are none above the level for that storm.

8. Summary of findings

Previous studies showed that FORTE observes RF signals from intracloud processes that are distributed between two extremes: Weak, polarized, narrow, and coherent pulses are one extreme, and are related to progressive leader breakdown. Strong, incoherent, and broader pulses are the other extreme, and to the extent that they can be associated with any other process, that process leads in some cases to Narrow Bipolar Events.

Here we have presented a statistical analysis of FORTE RF recordings of IC lightning activity, focusing on the relationship between strong RF emissions and other RF signals in either the same flash or the same storm. We have found:

- (a) ERP ~ 40 kW (referenced to the FORTE low band 26-48 MHz) appears to be an approximate dividing region, on different sides of which FORTE IC pulses have distinctive behaviors. Those on the lower side with ERP $\ll 40$ kW are the weak, polarized, narrow, and coherent pulses, while those on the higher side with ERP > 40 kW are the broader and incoherent “strong IC pulses”.
- (b) Strong IC pulses either occur singly (not in flashes), or initiate flashes. Strong IC pulses never occur within the interior of flashes.
- (c) The ERP of strong IC pulses exceeds the ERP of weak, polarized, narrow, and coherent pulses by 10^2 to 10^3 .

- (d) Strong IC pulses tend not to have optical concurrence. Almost all optical concurrence of RF IC pulses occurs for lower ERP pulses that are weak, polarized, narrow, and coherent.
- (e) Strong RF pulses can be concurrent with Narrow Bipolar Events seen by the Edot field-change array.
- (f) In storms that produce both strong RF pulses recorded by FORTE and NBE field changes recorded by Edot, there are always more strong RF pulses than NBEs. It appears that strong RF pulses can occur without an NBE, but not vice versa.
- (g) In storms containing both strong RF pulses recorded by FORTE and NBE field changes recorded by Edot, there are few if any flashes.
- (h) In storms containing flashes that are initiated by strong RF pulses, there are almost never NBEs.
- (i) In flashes that are initiated by strong RF pulses, the subsequent leader-like pulses in the flash tend to occur at higher altitude than where the flash is initiated.
- (j) In flashes that are initiated by strong RF pulses, optical concurrence (if it occurs at all) tends to occur only for subsequent pulses, and tends not to occur for the initiator strong RF pulse.
- (k) The optical::RF power ratio for weak, polarized, narrow, and coherent pulses exceeds the optical::RF output ratio for strong RF pulses by a factor of 10^2 or greater.
- (l) The strong RF pulses in a given storm appear to have a truncated ERP distribution, staying below a limiting ERP. For most storms this ERP limit is on the order of 1 MW in the FORTE low band 26-48 MHz.

9. Discussion

The behavior of strong RF IC pulses is no less enigmatic than the behavior of Narrow Bipolar Events [*Smith et al.*, 1999], and the two are related. We now speculate on a physical scenario that could underly both of these phenomena. The speculation is purely heuristic.

We infer from this study that strong RF emissions could not be generated by a thermalized gas/plasma equilibrium as occurs in leader segments [*Gallimberti*, 1979]. If the strong RF emissions came from a leader-like process, we would not expect such a gross disparity in the optical::RF power ratio. If on the other hand the strong RF emissions were associated with a discharge carried by superthermal electrons moving through a cold background gas, then the fluorescence would be much weaker than a leader's thermal line radiation.

Therefore we hypothesize that the strong RF emissions are related to a discharge carried by superthermal electrons which are somehow seeded and amplified in just a few microseconds. Since all known leader processes are much too slow to accomplish this [*Gallimberti*, 1979] over a relevant kilometer-scale E-field region, we hypothesize that the superthermal electron population must be seeded and amplified by a process unrelated to leaders.

We note that the large-scale charge transfer marked by an NBE field-change signal does not always accompany a strong RF pulse. This suggests that the RF pulse is a detail of the process of seeding and amplifying the superthermal electron population, and but that the final closure of the gap between charge regions does not always succeed. If the gap is not closed, then the charge distribution is not much changed, and the electric field remains largely unrelaxed.

We note that the strong RF pulse, *when it does not result in an NBE*, can nonetheless serve as the initiator of what appears to be a negative leader. We note further that the negative leader never occurs when the strong RF pulse is accompanied by an NBE. We know that a leader can occur only in a high external electric field. These facts are consistent with the notion that the strong RF pulse is emitted by a process which is necessary, but not sufficient, for the electric field to be subsequently relaxed as indicated by the NBE field-change. These facts are also consistent with the logic that if a leader is initiated by a strong RF event, then the electric field has not been effectively relaxed.

Gurevich, Zybin, and Roussel-Dupré [1999] have sketched a multi-step mechanism whereby a peta-eV (10^{15} eV) cosmic ray can instigate a large-scale IC discharge in microseconds rather than at leader timescales. The GZR process combines (a) a pre-existing, “external” thunderstorm electric field, (b) the massive infusion of secondary electrons, with a front advancing at the speed of light, in a PeV primary’s atmospheric shower, (c) the prior discovery of lowered-electric-field-threshold, electron-avalanche breakdown for relativistic electrons [Roussel-Dupré and Gurevich, 1996], and (d) a polarization of the conducting ionization structure and subsequent field enhancement at its tip. There is a ready supply (>1 /km²/s) of incident cosmic rays of sufficient energy for the GZR scenario, if its physics is valid, to occur. If we assume that a typical thunderstorm charge region is ~ 5 km in width, then the number of cosmic rays of sufficient energy striking this charge region is ~ 25 /s, which is much higher than the rate at which FORTE observes strong RF IC pulses in any given storm (typically on the order of 1-3 /s). The FORTE-observed rates of occurrence of strong RF IC pulses therefore do not contravene the upper limit that would be imposed by the available flux of suitable cosmic rays.

Acknowledgements

This work has been performed under the auspices of the U. S. Department of Energy, in a Laboratory Directed Research and Development project for the study of RF emissions instigated by cosmic-ray showers. The author is grateful to Drs. David Smith, Tracy Light, David Suszcynsky, John Willett, Ronald Thomas, Robert Roussel-Dupré, Peter Gorham, and Paul Krehbiel for useful discussions.

References

- Boccippio, D.J., S.J. Goodman, and S. Heckman, Regional differences in tropical lightning distributions, *J. Appl. Meteor.*, 39, 2231-2248, 2000.
- Boccippio, D.J., W.J. Koshak, H.J. Christian, and S.J. Goodman, Land-ocean differences in LIS and OTD tropical lightning observations, in *11th International Conference on Atmospheric Electricity*, edited by H. Christian, pp. 734-737, National Aeronautics and Space Administration (U. S.), Huntsville, Alabama, 1999.
- Christian, H.J., R.J. Blakeslee, D.J. Boccippio, W.L. Boeck, D.E. Buechler, K.T. Driscoll, S.J. Goodman, J.M. Hall, W.J. Koshak, D.M. Mach, and M.F. Stewart, Global frequency and distribution of lightning as observed by the Optical Transient Detector (OTD), in *11th International Conference on Atmospheric Electricity*, edited by H. Christian, pp. 726-729, National Aeronautics and Space Administration (U. S.), Huntsville, Alabama, 1999a.
- Christian, H.J., R.J. Blakeslee, S.J. Goodman, D.A. Mach, M.F. Stewart, D.E. Buechler, W.J. Koshak, J.M. Hall, W.L. Boeck, K.T. Driscoll, and D.J. Boccippio, The Lightning Imaging Sensor, in *11th International Conference on Atmospheric Electricity*, edited by H. Christian, NASA, Global Hydrology and Climate Center, NASA Marshall Space Flight Center, Huntsville, Alabama, 1999b.
- Gallimberti, I., The mechanism of the long spark formation, *Journal de Physique*, 40 (7), C7: 193-250, 1979.
- Gurevich, A.V., K.P. Zybin, and R.A. Roussel-Dupré, Lightning initiation by simultaneous effect of runaway breakdown and cosmic ray showers, *Phys. Lett.*, A254, 79-87, 1999.
- Heavner, M.J., D.A. Smith, A.R. Jacobson, and R.J. Sheldon, LF/VLF and VHF lightning fast-stepped leader observations, *J. Geophys. Res.*, 107 (D24), 4791, doi: 10.1029/2001JD001290, 2002.
- Jacobson, A.R., Relationship of intracloud-lightning radiofrequency power to lightning-storm height, as observed by the FORTE satellite, *J. Geophys. Res.*, in press, 2003.
- Jacobson, A.R., K.L. Cummins, M. Carter, P. Klingner, D. Roussel-Dupré, and S.O. Knox, FORTE radio-frequency observations of lightning strokes detected by the National Lightning Detection Network, *J. Geophys. Res.*, 105 (D12), 15,653, 2000.
- Jacobson, A.R., S.O. Knox, R. Franz, and D.C. Enemark, FORTE observations of lightning radio-frequency signatures: Capabilities and basic results, *Radio Sci.*, 34 (2), 337-354, 1999.
- Jacobson, A.R., and T.E.L. Light, Bimodal radiofrequency pulse distribution of intracloud-lightning signals recorded by the FORTE satellite, *J. Geophys. Res.*, in press, 2003.
- Jacobson, A.R., and X.-M. Shao, Using geomagnetic birefringence to locate sources of impulsive, terrestrial VHF signals detected by satellites on orbit, *Radio Sci.*, 36 (4), 671-680, 2001.
- Jacobson, A.R., and X.-M. Shao, FORTE satellite observations of very narrow radiofrequency pulses associated with the initiation of negative cloud-to-ground lightning strokes, *J. Geophys. Res.*, 107 (D22), 4661, doi:10.1029/2001JD001542, 2002a.

- Jacobson, A.R., and X.-M. Shao, On-orbit direction-finding of lightning radio-frequency emissions recorded by the FORTE satellite, *Radio Sci.*, 37 (4), 10.1029/2001RS002510, 2002b.
- Kirkland, M.W., D.M. Suszcynsky, J.L.L. Guillen, and J.L. Green, Observations of terrestrial lightning at optical wavelengths by the the FORTE satellite photodiode detector, *J. Geophys. Res.*, 106 (D24), 33,499-33,509, 2001.
- Le Vine, D.M., Sources of the strongest rf radiation from lightning, *J. Geophys. Res.*, 85 (C7), 4091-4095, 1980.
- Lee, A.C.L., An operational system for the remote location of lightning flashes using a VLF arrival time difference technique, *J. Atmos. Oceanic Technol.*, 3, 630-642, 1986.
- Light, T.E., D.M. Suszcynsky, and A.R. Jacobson, Coincident Radio Frequency and Optical Emissions from Lightning, Observed with the FORTE Satellite, *J. Geophys. Res.*, 106 (D22), 28,223-28,231, 2001.
- Light, T.E.L., and A.R. Jacobson, Characteristics of impulsive VHF lightning observed by the FORTE satellite, *J. Geophys. Res.*, in press, 2003.
- Massey, R.S., S.O. Knox, R.C. Franz, D.N. Holden, and C.T. Rhodes, Measurements of transionospheric radio propagation parameters using the FORTE satellite, *Radio Sci.*, 33 (6), 1739-1753, 1998.
- Rison, W., R.J. Thomas, P.R. Krehbiel, T. Hamlin, and J. Harlin, A GPS-based three-dimensional lightning mapping system: Initial observations in central New Mexico, *Geophys. Res. Lett.*, 26, 3573-3576, 1999.
- Roussel-Dupré, R., and A.V. Gurevich, On runaway breakdown and upward propagating discharges, *J. Geophys. Res.*, 101 (A2), 2297-2311, 1996.
- Roussel-Dupré, R.A., A.R. Jacobson, and L.A. Triplett, Analysis of FORTE data to extract ionospheric parameters, *Radio Sci.*, 36 (6), 1615-1630, 2001.
- Smith, D.A., K.B. Eack, J. Harlin, M.J. Heavner, A.R. Jacobson, R.S. Massey, X.M. Shao, and K.C. Wiens, The Los Alamos Sferic Array: A research tool for lightning investigations, *J. Geophys. Res.*, 107 (D13), 10.1029/2001JD000502, 2002.
- Smith, D.A., X.M. Shao, D.N. Holden, C.T. Rhodes, M. Brook, P.R. Krehbiel, M. Stanley, W. Rison, and R.J. Thomas, A distinct class of isolated intracloud lightning discharges and their associated radio emissions, *J. Geophys. Res.*, 104 (D4), 4189-4212, 1999.
- Suszcynsky, D., A. Jacobson, J. Fitzgerald, C. Rhodes, E. Tech, and D. Roussel-Dupre, Satellite-based global lightning and severe storm monitoring using VHF receivers, *EOS, Trans. Am. Geophys. Union*, 81 (48), F91, 2000a.
- Suszcynsky, D.M., M.W. Kirkland, A.R. Jacobson, R.C. Franz, S.O. Knox, J.L.L. Guillen, and J.L. Green, FORTE observations of simultaneous VHF and optical emissions from lightning: Basic Phenomenology, *J. Geophys. Res.*, 105 (D2), 2191-2201, 2000b.
- Suszcynsky, D.M., T.E. Light, S. Davis, M.W. Kirkland, J.L. Green, and J. Guillen, Coordinated Observations of Optical Lightning from Space using the FORTE Photodiode Detector and CCD Imager, *J. Geophys. Res.*, 106 (D16), 17,897-17,906, 2000c.

- Thomas, R.J., P.R. Krehbiel, W. Rison, T. Hamlin, J. Harlin, and D. Shown, Observations of VHF source powers radiated by lightning, *Geophys. Res. Lett.*, 28 (1), 143-146, 2001.
- Tierney, H., A.R. Jacobson, W.H. Beasley, and P.E. Argo, Determination of source thunderstorms for VHF emissions observed by the FORTE satellite, *Radio Sci.*, 36 (1), 79-96, 2001.
- Willett, J.C., J.C. Bailey, and E.P. Krider, A class of unusual lightning electric field waveforms with very strong high-frequency radiation, *J. Geophys. Res.*, 94 (D13), 16255-16267, 1989.
- Williams, E.R., Chapter 13: The Electrification of Severe Storms, in *Severe Convective Storms*, edited by C.A.I. Doswell, American Meteorological Society, 2001.